Chapter II

Electron cryotomography of the *E. coli* pyruvate and 2-oxoglutarate dehydrogenase complexes

Gavin E. Murphy, Grant J. Jensen*

Division of Biology, California Institute of Technology, Pasadena, CA 91125, USA

*Correspondence: 1200 E. California Blvd., Pasadena, CA 91125, 626-395-8827 (phone), 626-395-5730 (fax), Jensen@caltech.edu.

Published in Structure 2005 Dec; 13(12):1765-73.

doi: 10.1016/j.str.2005.08.01

Received 27 May 2005; revised 27 July 2005; accepted 1 August 2005. Published: December 13, 2005. Available online 13 December 2005.

Summary

The *E. coli* pyruvate and 2-oxoglutarate dehydrogenases are two closely related, large complexes that exemplify a growing number of multiprotein "machines" whose domains have been studied extensively and modeled in atomic detail, but whose quaternary structures have remained unclear for lack of an effective imaging technology. Here, electron cryotomography was used to show that the E1 and E3 subunits of these complexes are flexibly tethered ~ 11 nm away from the E2 core. This result demonstrates unambiguously that electron cryotomography can reveal the relative positions of features as small as 80 kDa in *individual* complexes, elucidating quaternary structure and conformational flexibility.

Introduction

The pyruvate and 2-oxoglutarate dehydrogenases of *E. coli* (PDHC and OGDHC, respectively) are two closely related assemblies of three protein types each (E1, E2, and E3). Together, the three enzymes catalyze five separate reactions that in sum decarboxylate 2-oxo acids and attach the remaining acyl group to coenzyme A (de Kok et al., 1998). PDHC converts pyruvate to acetyl-CoA, which then enters the citric acid cycle. OGDHC acts within the citric acid cycle, converting 2-oxoglutarate to succinyl-CoA. The E2 polypeptide (dihydrolipoamide acetyltransferase or dihydrolipoamide succinate transferase in PDHC and OGDHC, respectively) contains an ~ 26 kDa catalytic domain, an ~ 4 kDa E1/E3 binding domain, and either three or one (in PDHC and OGDHC, respectively) ~ 8 kDa lipoyl domains. Each of these domains is separated by apparently flexible "tether" sequences rich in alanine and proline and exposed to solvent (de Kok et al., 1998; Green et al., 1992; Perham, 1991). In both PDHC and OGDHC, the catalytic domains of 24 copies of E2 unite to form an octahedral "core" at the center of the complex. Outside this core, dimers of both the E3 (dihydrolipoamide dehydrogenase) and E1 (pyruvate dehydrogenase or 2-oxoglutarate dehydrogenase in PDHC and OGDHC, respectively) enzymes bind to E2's E1/E3 binding domain. In contrast, eukaryotic PDHC is icosahedral with a core made up of 60 E2s arranged as a pentagonal dodecahedron, 12 E3s bound within the pentagonal openings, and E1s bound peripherally through a flexible linker on E2 (Gu et al., 2003; Zhou et al., 2001a). In the reaction cycle, the 2-oxo acid is captured and decarboxylated by an E1 and then transferred to the mobile lipoyl domain of an E2. The lipoyl domain carries the acyl group to E2's catalytic

domain, which transfers it to coenzyme A. Acyl-CoA is released, and the lipoyl domain of E2 is regenerated (reoxidized) for another cycle by E3.

Following decades of study, atomic models for all the ordered domains of E1, E2, and E3 are now available, either directly or by homology to a closely related structure (Arjunan et al., 2002; Hendle et al., 1995; Jones et al., 2000; Mande et al., 1996). PDHC can accommodate up to 24 dimers of either E1 alone or E3 alone, and these compete for binding when mixed (Reed et al., 1975). The E1:E2:E3 chain ratio of the wild-type PDHC complex has been measured variously as 1:1:1, 2:2:1, 2:1:1, and 4:3:2 (Bosma et al., 1984; de Kok et al., 1998; Reed et al., 1975), apparently due to differing preparation and measurement methods.

Three lines of evidence led to the so-called "face/edge" model for the quaternary structure in which one E1 dimer binds to each of the 12 edges of the E2 core and one E3 dimer binds to each of the 6 faces, with the lipoyl domains moving freely above and between them. First, early experiments indicated that the highest rates of catalysis occurred with chain ratios of 2:2:1, which matches the numbers of faces and edges of a cube (Reed et al., 1975). Second, EM images of negatively stained samples, including intact and trypsin-treated PDHC complexes, as well as E2 cores, were judged to support the face/edge model, though some flexibility was suggested for the interaction of E1 with E2 (Bleile et al., 1979; Oliver and Reed, 1982). Finally, STEM images of several lyophilized and cross-linked samples, including PDHC, an E2-E3 subcomplex, and the E2 core, were used to generate radial density plots (Yang et al., 1985). Compared to the E2 core, the E2-E3 subcomplex had more mass from 0 to 11 nm. PDHC had more mass than the subcomplex from 8 to 22 nm. Because the E2 core extends up to 8 nm from the

center, and the E1 and E3 dimers have diameters of approximately 9 nm, the authors interpreted their results as supportive of the face/edge model.

A more distant and flexible attachment of the subunits to the core was shown by electron cryomicroscopy images of PDHC and OGDHC (Wagenknecht et al., 1992; Wagenknecht et al., 1990). For PDHCs loaded with either E1 or E3 separately, gaps of 4–6 and 3–4 nm were observed between the E2 core and the extra density attributed to E1 or E3, respectively. Similarly, for OGDHC, gaps of 2–4 and 3–5 nm were observed. The average distance from the center of the subunits to the center of the core was judged to be ~ 13 nm (Wagenknecht et al., 1992). The highly variable contrast extending 14–16 nm from the core's surface was attributed to the lipoyl domains. Despite this electron cryomicroscopy data supporting a flexible and extended nature of the complexes, the face/edge model has not been discarded, although it has been qualified that such a model is merely a time-averaged structure, and that the E3 subunits may be mobile (de Kok et al., 1998). Other techniques, including fluorescence energy transfer—which showed that the distance between the E1 and E3 active sites was between 3 and 6 nm—have not distinguished between the models (Moe et al., 1974). Thus PDHC and OGDHC are examples of a growing number of large macromolecular "machines" where atomic models of all the subunits are available, but the quaternary structure of the complete complex remains unclear, probably because the machine is inherently flexible or too difficult to purify to homogeneity for study by traditional means.

In order to clarify the molecular organization of these dehydrogenases, electron cryotomography was performed. In this technique, projections of a frozen sample are recorded with an electron microscope as it is tilted about one or two axes (Baumeister et

al., 1999). Thus while other standard structural biology techniques such as X-ray crystallography, NMR spectroscopy, electron crystallography, and electron cryomicroscopy-based single particle analysis all require averaging signals from large numbers of identical copies of the object of interest, electron cryotomography can be used to determine three-dimensional structures of *unique* objects ranging from whole cells to individual protein complexes. While the idea is several decades old, because the necessary instruments and protocols for this technique have only recently (~ 1997) became available, only a couple dozen applications have been published to date [for recent reviews, see (Kürner et al., 2004; McIntosh et al., 2005; Subramaniam and Milne, 2004)]. Nevertheless, these have already achieved resolutions sufficient to recognize membranes, protein shells, filaments, and some individual protein complexes. Among those that have targeted purified protein complexes (Bohm et al., 2000; Frangakis et al., 2002; Medalia et al., 2002; Nitsch et al., 1998; Sandin et al., 2004; Walz et al., 1997; Zhao et al., 2004), it has already been shown that tomographic reconstructions of individual particles are clear enough to be mutually aligned and averaged, and that different species mixed together in the same reconstruction can be distinguished computationally. It has long been hoped, however, that electron cryotomography would eventually reveal the structure of *individual* particles to high enough resolution that atomic models of subunits could simply be "docked," yielding both quaternary structure and conformational variability between particles. Indeed one recent study claimed to have done just that (Sandin et al., 2004) using small underfocuses and doses followed by extensive denoising. The reliability of the results was unclear, however, because (1) the shapes of specific domains were changed significantly by the denoising; (2) only a small

percentage of the appropriately-sized densities were then described as having "well-resolved subunits," and (3) all the remaining variability seen in this small, chosen class was attributed to conformational heterogeneity in the particles themselves, rather than as an inherent resolution limitation or an artifact of denoising.

Here a different strategy has been explored using higher defocuses and doses, but then no denoising. Dual-axis tilt-series (Iancu et al., 2005) were also used for the first time for purified protein complexes. The results are noteworthy as individual, ~ 80 kDa features within both the PDHC and OGDHC core are clearly discernible *without any averaging or denoising*; their relative positions are reproduced in many independent particles; and these positions match the known core structure well. The resolution was insufficient, however, to dock the crystal structures of the peripheral domains uniquely. Nevertheless, the results show clearly that in PDHC and ODGHC, the E1 and E3 subunits are flexibly tethered ~ 11 nm away from the E2 core.

Results

Solutions of purified PDHC and OGDHC were plunge-frozen in thin films across EM grids. Orthogonal dual-axis tilt-series (Iancu et al., 2005) were recorded through many holes in the carbon support, aligned, and merged to produce three-dimensional reconstructions of fields of particles suspended in vitreous ice. In the individual low-dose images of the tilt-series, particles were quite faint and barely recognizable (Fig. II-1a). After the reconstruction process, the complexes stood out unambiguously from the background (Fig. II-1b). All eight ~ 80 kDa corners of the E2 core were often visible in serial x-y slices of extracted, unaveraged, undenoised, and unrefined particles in which

only in-plane rotations had been performed. Their arrangement matched the low-pass-filtered E2 core crystal structure well, as could be most easily judged when the particles froze with their 4-, 3-, or 2-fold axes perpendicular to the grid (Fig. II-1c–j). The resolution was estimated to be ~5.5 nm using the Fourier Shell Correlation method. The globular nature of the peripheral subunits and their separation from the E2 core were also clear (Fig. II-2), demonstrating conclusively that the E1 and E3 subunits are indeed flexibly attached some distance away from the core, rather than bound specifically to the faces and edges. The asymmetric and non-homogenous nature of the *E. coli* PDHC prevented meaningful classification and averaging, as was done for the eukaryotic PDHC (Gu et al., 2003).

To distinguish between the face/edge and flexibly-tethered models quantitatively, their radial densities were compared to those of several individual, reconstructed particles (Fig. II-3). The radial density of the E2 core X-ray crystal structure shows a single peak at ~ 5 nm from the center. A face/edge model was built by placing 12 E1 dimers along the edges and 6 E3 dimers on the faces of the E2 core. The radial density of this model shows two peaks: the same peak at ~ 5 nm due to the E2 core, and another at ~ 10 nm from the additional E1/E3 subunits. To compare these to the experimentally reconstructed PDHC and OGDHC particles, the raw densities in the reconstructions were scaled linearly to match the atomic models at the top of the ~ 5 nm peak and decay to zero density at the edge of the reconstructed volumes. The experimentally reconstructed particles have two density peaks at ~ 5 and ~ 16 nm, separated by a clear minimum at ~ 10 nm. The "negative" densities at the origin, ~ 10 nm and ~ 25 nm in these plots, are artifacts of the point-spread-function, which under our imaging conditions looks roughly

like a sinc function with the first minima ~ 6 nm away from the center. This interpretation was confirmed by the radial density profiles of the 10 nm gold fiducials, which also show minima 6–8 nm away from their density peaks. Finally, the radial density of a fitted model of PDHC (described later) was plotted which matched the experimental densities well. Together these curves argue definitively for the flexibly-tethered model and highlight the reproducibility of the tomographic reconstructions.

Three hundred and five PDHC particles were selected from the reconstructions and aligned to the E2 crystal structure. Due to the regular configuration of the 24 E2 catalytic domains in PDHC, this alignment was straightforward and unambiguous. Next we tried to dock the structures of E1 and E3 into the peripheral densities in several reconstructions using the Situs software (Wriggers and Birmanns, 2001). Unfortunately, the peripheral tomographic densities did not partition clearly into two classes, which could potentially have corresponded to the ~ 100 kDa E3 dimer and the ~ 200 kDa E1 dimer. Thus, which peripheral densities were E1 and which were E3 could not be distinguished. This was particularly true where multiple subunits were close together or touching, yielding continuous reconstructed densities large enough to accommodate more than one E1 or E3 dimer. This fact illustrates how *distinguishing subunits* by shape or size requires higher resolution than simply *resolving their separate positions*, as was possible with the ~ 80 kDa corners of the E2 core. Nevertheless, to explore the range of positions accessible to E1/E3 subunits, three reconstructed PDHC particles (the three rendered in Fig. II-2) were thresholded so as to enclose a volume corresponding to a fully-loaded complex and crystal structures were roughly placed into the densities (Fig.

II-4). In the three interpreted structures, 24, 23 and 21 peripheral subunits could be positioned with a plausible correspondence to the surface map.

The positions of each fitted E1/E3 subunit were displayed in the same space as an averaged, octahedrally symmetrized map generated from all 305 PDHC particles (Fig. II-5a). No pattern was discerned in the positions of the E1/E3 subunits. To investigate further, the 8 corners of the core were superimposed, moving each fitted subunit accordingly to preserve its relationship to the corner. A new coordinate system was established wherein the three-fold axis of the corner was defined as the z-axis, the tip of the corner (defined by the center of the three most N-terminal residues of the E2 trimer) was defined as the origin, and the direction of the x-axis was left arbitrary. In this way the distance, relative azimuthal angle, and polar angle of the subunits' center-of-mass could be observed in relation to the corner. First, the distribution of relative azimuthal angles was displayed by rotating each subunits' center-of-mass onto the x-y plane (i.e. its polar angle was increased to 90˚). The azimuthal angle was apparently random (Fig. II-5b). Next, each center-of-mass was rotated onto the x-z plane (Fig. II-5c). The minimum, maximum, and average polar angle were 7˚, 70˚, and 41º (standard deviation 15º). The minimum, maximum, and mean distance between the corner and the subunits' centers-of-mass were 6.8, 15, and 11 nm (standard deviation 1.9 nm). Similar results were obtained for OGDHC.

Discussion

This paper reports two key findings. The first is of interest primarily to the enzymology community: that in the pyruvate and 2-oxoglutarate dehydrogenase

multienzyme complexes of *E. coli* (PDHC and OGDHC, respectively), the E1 and E3 enzymes are flexibly tethered ~ 11 nm away from the E2 core, rather than being specifically bound to the faces or edges. The second finding is of broad interest to the cell and structural biology communities: that electron cryotomography can reveal the quaternary structure and conformation of *individual* multiprotein complexes with resolutions sufficient to visualize the relative locations of features as small as 80 kDa.

Concerning the conformation of PDHC and OGDHC, the measurements of distance, azimuthal angle, and polar angle of the fitted subunits with respect to their closest corner are consistent with the hypothesis that E1 and E3 diffuse freely, constrained only by the length of their tether and steric occlusion. If the 31-residue tether between the catalytic and E1/E3 binding domains of E2 were fully extended (0.38 nm/residue), for instance, its maximum expected length would be 12 nm (blue circle in Fig. II-5). Adding the ~ 4.5 nm radius of an E1 or E3 subunit, the largest distance expected between a corner and the center-of-mass of an E1 or E3 would be ~ 16 nm, and indeed our measured maximum (15 nm) was just below that value. If the tether is assumed to be completely flexible and adopt a random-walk configuration, its expected length would be $(8/3\pi)^{1/2} N^{1/2} b$, where N is the number of steps (residues) and b is the length of one step (0.38 nm/residue) (Boal, 2002). This leads to an expected length of only 2.0 nm (purple circle in Fig. II-5). This value is too small, however, to accommodate more than just a few E1 and E3 dimers in the complete assembly. Thus the average distance of 11 nm measured here (corresponding to a tether length of ~ 6 nm, assuming the tether is usually attached to an inner-facing surface of E1 or E3) is reasonable, as it lies between these two extremes. A 9-nm thick spherical shell

(corresponding to the approximate diameter of an E1 or E3 subunit) centered on PDHC at a radius 11 nm past a corner (the average distance observed here) has a volume ~ 4.5 times larger than a full complement of 16 E1 and 8 E3 dimers. Thus this distance is also plausible for mobile and colliding subunits tethered to a common point. Concerning the polar angle, if three spheres of radius 4.5 nm are placed 11 nm away from a corner so that they just touch, their polar angles would be 29˚. The measured average of 41˚ is comfortably larger than that minimum, but no values past 70˚ are seen, since such angles would place subunits deep into the already occupied space above adjacent corners.

These results can be compared to those obtained for the eukaryotic forms of PDHC (Zhou et al., 2001b). In *Saccharomyces cerevisiae* PDHC, the E2 core is icosahedral, but expands and contracts uniformly by ~ 20%. It has been proposed that this "breathing" is thermally driven, and may augment the movement of substrates between active sites. Here no significant variation in the E2 core dimensions was measured, as predicted, because of the additional inter-trimer interactions in the *E. coli* PDHC (Zhou et al., 2001a). In the presence of substoichiometric amounts of E1, the *S. cerevisiae* E1 shell appears to be icosahedrally ordered. More complete occupancy of E1 lengthens the linker between E1 and E2 from ~ 5.0 to ~ 7.5 nm and disrupts the symmetry of the E1 shell (Gu et al., 2003). Here no evidence was found for order in the E1/E3 shell or for any preferred conformations of the ~ 11 nm linker.

In order to obtain an intuitive sense for the length of the tethers and the crowdedness within PDHC and OGDHC, and to present our flexible model visually as an alternative to the traditional face/edge model, a complete atomic model of one corner was assembled (Fig. II-6). The crystal structure for E2 was used as a starting point (Hendle

et al., 1995). A crystal structure of an E3 dimer in complex with E2's E1/E3 binding domain (Mande et al., 1996) was then fit into the three main peripheral densities seen surrounding a corner of one reconstructed PDHC. E1 was not used because there is no crystal structure available of it specifically bound to the E1/E3 binding domain. The 31-residue tether present in the E2 sequence between the catalytic and E1/E3 binding domains was modeled as a beta-strand and positioned accordingly. Finally, an NMR structure of the lipoyl domain (Jones et al., 2000) was placed at nine reasonable but purely hypothetical locations (three for each of the three E2 monomers that form the corner). The nine corresponding tether sequences were modeled between them mostly as an extended beta-strand, except wherever there was a strong secondary-structure prediction for a helix. (A schematic figure in (Aevarsson et al., 1999) previously illustrated the relative size of the components and the reaction cycle, but the length of the linkers and the crowdedness of the complex were not meant to be physically realistic.) This complete model revealed that there is still sufficient space around the subunits for the tethers and lipoyl domains to move. Given that each corner has three E2 monomers, that the E1/E3 binding domains can bind either E1 or E3, and that these subunits are flexibly tethered several nanometers away from the corner, then the entire complex is inherently nonhomogeneous, asymmetric, and flexible.

The ultimate potential of electron cryotomography is, of course, still unknown. In this study, relatively high total doses (~ 120 e^-/A^2) and high defocus values (–10 μm) were used in an effort to obtain the most interpretable reconstructions possible *without the use of any post-processing (denoising)*, which can introduce artifacts. In a comparable study (Sandin et al., 2004), much lower doses and defocus values were used,

but the reconstructions only became interpretable after extensive denoising, and the reliability of the final results was difficult to assess. Further studies are needed to determine how faithful the various denoising techniques actually are and how to optimally balance radiation damage, contrast enhancement through defocus, and denoising. Nevertheless, electron cryotomography has unambiguously demonstrated here its capacity to reveal quaternary structure and conformational variability, and should be applied generally to the myriad large, multi-protein machines found in nature.

Experimental Procedures

Sample Preparation

Unengineered PDHC and OGDHC were purified from *E. coli* and assayed for activity as described (Wagenknecht et al., 1992). Carbon-coated, R1.5/1.3 Quantifoil grids (Quantifoil Micro Tools GmbH) were glow-discharged and treated with 5 μL of 10 nm colloidal gold (Ted Pella). Purified protein was diluted to 2 mg/ml in 20 mM potassium phosphate buffer pH 7.0, and additional gold was added. Four-μL samples at 22˚ C were plunge-frozen using a Vitrobot (FEI Company) in 100% humidity using a 3.5 s blot time and a –3 offset. Frozen grids were stored in liquid nitrogen.

Cryo-electron tomography

Grids were mounted into “flip-flop” cartridges (Iancu et al., 2005) and imaged with an FEI Polara FEG TEM cooled by liquid nitrogen. Orthogonal dual-axis tomographic tilt-series from -63° to 63° on both axes in steps of 3° were collected at 300 kV under low dose conditions on a Gatan imaging filter (20 eV slit width) using the UCSF tomography

package (Zheng et al., 2004). The magnification was 27,500 (0.82 nm/pixel), the defocus was –10 μm (first CTF zero at 1/4.5 nm^{-1}), and the total dose per sample was ~ 120 e^-/A^2, distributed according to the 1/cos scheme.

Image Processing

Dual-axis tomograms were reconstructed with IMOD using weighted back-projection (Mastronarde, 1997) and were low-pass filtered to the resolution of the first CTF zero. Individual particles are shown in Fig. II-2. Using the Bsoft package (Heymann, 2001) and the Peach distributed-computing system (Leong et al., 2005), 305 and 42 spherical volumes with radii of 40 nm (including individual PDHC and OGDHC particles, respectively) were extracted from the tomograms, aligned to the low-pass filtered crystal structure of the E2 core from either PDHC (PDB ID #1DPC) (Hendle et al., 1995) or OGDHC (PDB ID #1E2O) (Knapp et al., 1998), averaged, and symmetrized solely to produce the isosurface background of Fig. II-5. Only measured regions of reciprocal space were used to align the particles to the crystal structure (the missing pyramid was excluded in calculations of the cross correlation coefficient). A resolution of 5.5 nm was estimated using Fourier shell correlation (using the 0.5 threshold) by extracting the core from one individual aligned PDHC particle and correlating it with the 2.0 nm low-pass filtered, E2 crystal structure.

Modeling

Amira (Mercury Computer Systems) was used for all surface and volume rendering and segmentation. Individual reconstructions were thresholded to enclose a volume

corresponding to 5.6 MDa, which is the sum of 24 E2 monomers, 16 E1 dimers and 8 E3 dimers. This corresponds to an E1:E2:E3 chain ratio of 4:3:2, which was favored here among the various reported values because it saturates the E1/E3 binding sites and has been indicated by some measurements as the optimal stoichiometry (Bosma et al., 1984; de Kok et al., 1998; Reed et al., 1975). Crystal structures of E1 (PDB ID #1L8A) (Arjunan et al., 2002) and E3 subunits (PDB ID #1EBD) (Mande et al., 1996) were placed within peripheral densities as described. None of the conclusions depended on the exact threshold used because the gradients defining the peripheral densities in the reconstructions were steep and only the center positions of the fit crystal structures (rather than specific orientations) were used in the analysis. VMD (Humphrey et al., 1996) was used to visualize and manipulate the atomic models. Deep View (Guex and Peitsch, 1997) was used to build a hypothetical model of one complete corner of PDHC using the *A. vinelandii* E2 core (PDB ID #1DPC, 56% identity) (Hendle et al., 1995), E3 bound to the E1/E3 binding domain from *B. stearothermophilus* (PDB ID #1EBD, 44% identity) (Mande et al., 1996), the *E. coli* lipoyl domain (PDB ID #1QJO) (Jones et al., 2000), and tether sequences from *E. coli*. The 11 most N-terminal residues present in the *Azotobacter vinelandii* E2 core crystal structure are thought to be part of the 31-residue disordered tether in the *E. coli* complex (Bateman et al., 2004), and so were depicted as such here. One extracted PDHC particle and one OGDHC particle were submitted to the EM Data Bank with the accession codes EMD-1151 and EMD-1152, respectively.

Acknowledgements

We thank T. Wagenknecht and J. Berkowitz for the protein samples, and A. Rawlinson for help preparing the figures. This work was supported in part by NIH Grant PO1 GM66521 to GJJ, DOE grant DE-FG02-04ER63785 to GJJ, the Beckman Institute at Caltech, and gifts to Caltech from the Ralph M. Parsons Foundation, the Agouron Institute, and the Gordon and Betty Moore Foundation.

References

Aevarsson, A., Seger, K., Turley, S., Sokatch, J. R., and Hol, W. G. (1999). Crystal structure of 2-oxoisovalerate and dehydrogenase and the architecture of 2-oxo acid dehydrogenase multienzyme complexes. Nat. Struct. Biol. *6*, 785-792.

Arjunan, P., Nemeria, N., Brunskill, A., Chandrasekhar, K., Sax, M., Yan, Y., Jordan, F., Guest, J. R., and Furey, W. (2002). Structure of the pyruvate dehydrogenase multienzyme complex E1 component from Escherichia coli at 1.85 A resolution. Biochemistry *41*, 5213-5221.

Bateman, A., Coin, L., Durbin, R., Finn, R. D., Hollich, V., Griffiths-Jones, S., Khanna, A., Marshall, M., Moxon, S., Sonnhammer, E. L.*, et al.* (2004). The Pfam protein families database. Nucleic Acids Res. *32*, D138-141.

Baumeister, W., Grimm, R., and Walz, J. (1999). Electron tomography of molecules and cells. Trends Cell Biol. *9*, 81-85.

Bleile, D. M., Munk, P., Oliver, R. M., and Reed, L. J. (1979). Subunit structure of dihydrolipoyl transacetylase component of pyruvate dehydrogenase complex from Escherichia coli. Proc. Natl. Acad. Sci. U.S.A. *76*, 4385-4389.

Boal, D. (2002). Mechanics of the Cell (Cambridge, UK: Cambridge University Press).

Bohm, J., Frangakis, A. S., Hegerl, R., Nickell, S., Typke, D., and Baumeister, W. (2000). Toward detecting and identifying macromolecules in a cellular context: Template matching applied to electron tomograms. Proc. Natl. Acad. Sci. U.S.A. *97*, 14245-14250.

Bosma, H. J., de Kok, A., Westphal, A. H., and Veeger, C. (1984). The composition of the pyruvate dehydrogenase complex from Azotobacter vinelandii. Does a unifying model exist for the complexes from gram-negative bacteria? Eur. J. Biochem. *142*, 541-549.

de Kok, A., Hengeveld, A. F., Martin, A., and Westphal, A. H. (1998). The pyruvate dehydrogenase multi-enzyme complex from Gram-negative bacteria. Biochim. Biophys. Acta *1385*, 353-366.

Frangakis, A. S., Bohm, J., Forster, F., Nickell, S., Nicastro, D., Typke, D., Hegerl, R., and Baumeister, W. (2002). Identification of macromolecular complexes in cryoelectron tomograms of phantom cells. Proc. Natl. Acad. Sci. U.S.A. *99*, 14153-14158.

Green, J. D., Perham, R. N., Ullrich, S. J., and Appella, E. (1992). Conformational studies of the interdomain linker peptides in the dihydrolipoyl acetyltransferase component of the pyruvate dehydrogenase multienzyme complex of Escherichia coli. J. Biol. Chem. *267*, 23484-23488.

Gu, Y., Zhou, Z. H., McCarthy, D. B., Reed, L. J., and Stoops, J. K. (2003). 3D electron microscopy reveals the variable deposition and protein dynamics of the peripheral pyruvate dehydrogenase component about the core. Proc. Natl. Acad. Sci. U.S.A. *100*, 7015-7020.

Guex, N., and Peitsch, M. C. (1997). SWISS-MODEL and the Swiss-PdbViewer: an environment for comparative protein modeling. Electrophoresis *18*, 2714-2723.

Hendle, J., Mattevi, A., Westphal, A. H., Spee, J., de Kok, A., Teplyakov, A., and Hol, W. G. (1995). Crystallographic and enzymatic investigations on the role of Ser558, His610, and Asn614 in the catalytic mechanism of Azotobacter vinelandii dihydrolipoamide acetyltransferase (E2p). Biochemistry *34*, 4287-4298.

Heymann, J. B. (2001). Bsoft: image and molecular processing in electron microscopy. J. Struct. Biol. *133*, 156-169.

Humphrey, W., Dalke, A., and Schulten, K. (1996). VMD: visual molecular dynamics. J. Mol. Graphics *14*, 33-38, 27-38.

Iancu, C. V., Wright, E. R., Benjamin, J., Tivol, W. F., Dias, D. P., Murphy, G. E., Heymann, J. B., and Jensen, G. J. (2005) A "flip-flop" rotation stage for routine dual-axis electron cryotomography. J. Struct. Biol. *151,* 288-297.

Jones, D. D., Stott, K. M., Howard, M. J., and Perham, R. N. (2000). Restricted motion of the lipoyl-lysine swinging arm in the pyruvate dehydrogenase complex of Escherichia coli. Biochemistry *39*, 8448-8459.

Knapp, J. E., Mitchell, D. T., Yazdi, M. A., Ernst, S. R., Reed, L. J., and Hackert, M. L. (1998). Crystal structure of the truncated cubic core component of the Escherichia coli 2-oxoglutarate dehydrogenase multienzyme complex. J. Mol. Biol. *280*, 655-668.

Kürner, J., Medalia, O., Linaroudis, A. A., and Baumeister, W. (2004). New insights into the structural organization of eukaryotic and prokaryotic cytoskeletons using cryo-electron tomography. Exp. Cell Res. *301*, 38-42.

Leong, P. A., Heymann, J. B., and Jensen, G. J. (2005). Peach: A simple Perl-based system for distributed computation and its application to cryoEM data processing. Structure *13*, 1-7.

Mande, S. S., Sarfaty, S., Allen, M. D., Perham, R. N., and Hol, W. G. (1996). Protein-protein interactions in the pyruvate dehydrogenase multienzyme complex: dihydrolipoamide dehydrogenase complexed with the binding domain of dihydrolipoamide acetyltransferase. Structure *4*, 277-286.

Mastronarde, D. N. (1997). Dual-axis tomography: an approach with alignment methods that preserve resolution. J. Struct. Biol. *120*, 343-352.

McIntosh, R., Nicastro, D., and Mastronarde, D. (2005). New views of cells in 3D: an introduction to electron tomography. Trends Cell Biol. *15*, 43-51.

Medalia, O., Typke, D., Hegerl, R., Angenitzki, M., Sperling, J., and Sperling, R. (2002). Cryoelectron microscopy and cryoelectron tomography of the nuclear pre-mRNA processing machine. J. Struct. Biol. *138*, 74-84.

Moe, O. A., Jr., Lerner, D. A., and Hammes, G. G. (1974). Fluorescence energy transfer between the thiamine diphosphate and flavine adenine dinucleotide binding sites on the pyruvate dehydrogenase multienzyme complex. Biochemistry *13*, 2552-2557.

Nitsch, M., Walz, J., Typke, D., Klumpp, M., Essen, L. O., and Baumeister, W. (1998). Group II chaperonin in an open conformation examined by electron tomography. Nat. Struct. Biol. *5*, 855-857.

Oliver, R. M., and Reed, L. J. (1982). Multienzyme Complexes, In Electron Microscopy of Proteins, R. Harris, ed. (London: Academic Press), pp. 1-48.

Perham, R. N. (1991). Domains, motifs, and linkers in 2-oxo acid dehydrogenase multienzyme complexes: a paradigm in the design of a multifunctional protein. Biochemistry *30*, 8501-8512.

Reed, L. J., Pettit, F. H., Eley, M. H., Hamilton, L., Collins, J. H., and Oliver, R. M. (1975). Reconstitution of the Escherichia coli pyruvate dehydrogenase complex. Proc. Natl. Acad. Sci. U.S.A. *72*, 3068-3072.

Sandin, S., Ofverstedt, L. G., Wikstrom, A. C., Wrange, O., and Skoglund, U. (2004). Structure and flexibility of individual immunoglobulin G molecules in solution. Structure *12*, 409-415.

Subramaniam, S., and Milne, J. L. S. (2004). Three-dimensional electron microscopy at molecular resolution. Annu. Rev. Biophys. Biomol. Struct. *33*, 141-155.

Wagenknecht, T., Grassucci, R., Berkowitz, J., and Forneris, C. (1992). Configuration of interdomain linkers in pyruvate dehydrogenase complex of Escherichia coli as determined by cryoelectron microscopy. J. Struct. Biol. *109*, 70-77.

Wagenknecht, T., Grassucci, R., and Schaak, D. (1990). Cryoelectron microscopy of frozen-hydrated alpha-ketoacid dehydrogenase complexes from Escherichia coli. J. Biol. Chem. *265*, 22402-22408.

Walz, J., Tamura, T., Tamura, N., Grimm, R., Baumeister, W., and Koster, A. J. (1997). Tricorn protease exists as an icosahedral supermolecule in vivo. Mol. Cell *1*, 59-65.

Wriggers, W., and Birmanns, S. (2001). Using Situs for flexible and rigid-body fitting of multiresolution single-molecule data. J. Struct. Biol. *133*, 193-202.

Yang, H. C., Hainfeld, J. F., Wall, J. S., and Frey, P. A. (1985). Quaternary structure of pyruvate dehydrogenase complex from Escherichia coli. J. Biol. Chem. *260*, 16049-16051.

Zhao, Q., Ofverstedt, L. G., Skoglund, U., and Isaksson, L. A. (2004). Morphological variation of individual Escherichia coli 30S ribosomal subunits in vitro and in situ, as revealed by cryo-electron tomography. Exp. Cell Res. *297*, 495-507.

Zheng, Q. S., Braunfeld, M. B., Sedat, J. W., and Agard, D. A. (2004). An improved strategy for automated electron microscopic tomography. J. Struct. Biol. *147*, 91-101.

Zhou, Z. H., Liao, W., Cheng, R. H., Lawson, J. E., McCarthy, D. B., Reed, L. J., and Stoops, J. K. (2001a). Direct evidence for the size and conformational variability of the pyruvate dehydrogenase complex revealed by three-dimensional electron microscopy. The "breathing" core and its functional relationship to protein dynamics. J. Biol. Chem. *276*, 21704-21713.

Zhou, Z. H., McCarthy, D. B., O'Connor, C. M., Reed, L. J., and Stoops, J. K. (2001b). The remarkable structural and functional organization of the eukaryotic pyruvate dehydrogenase complexes. Proc. Natl. Acad. Sci. U.S.A. *98*, 14802-14807.

Figures

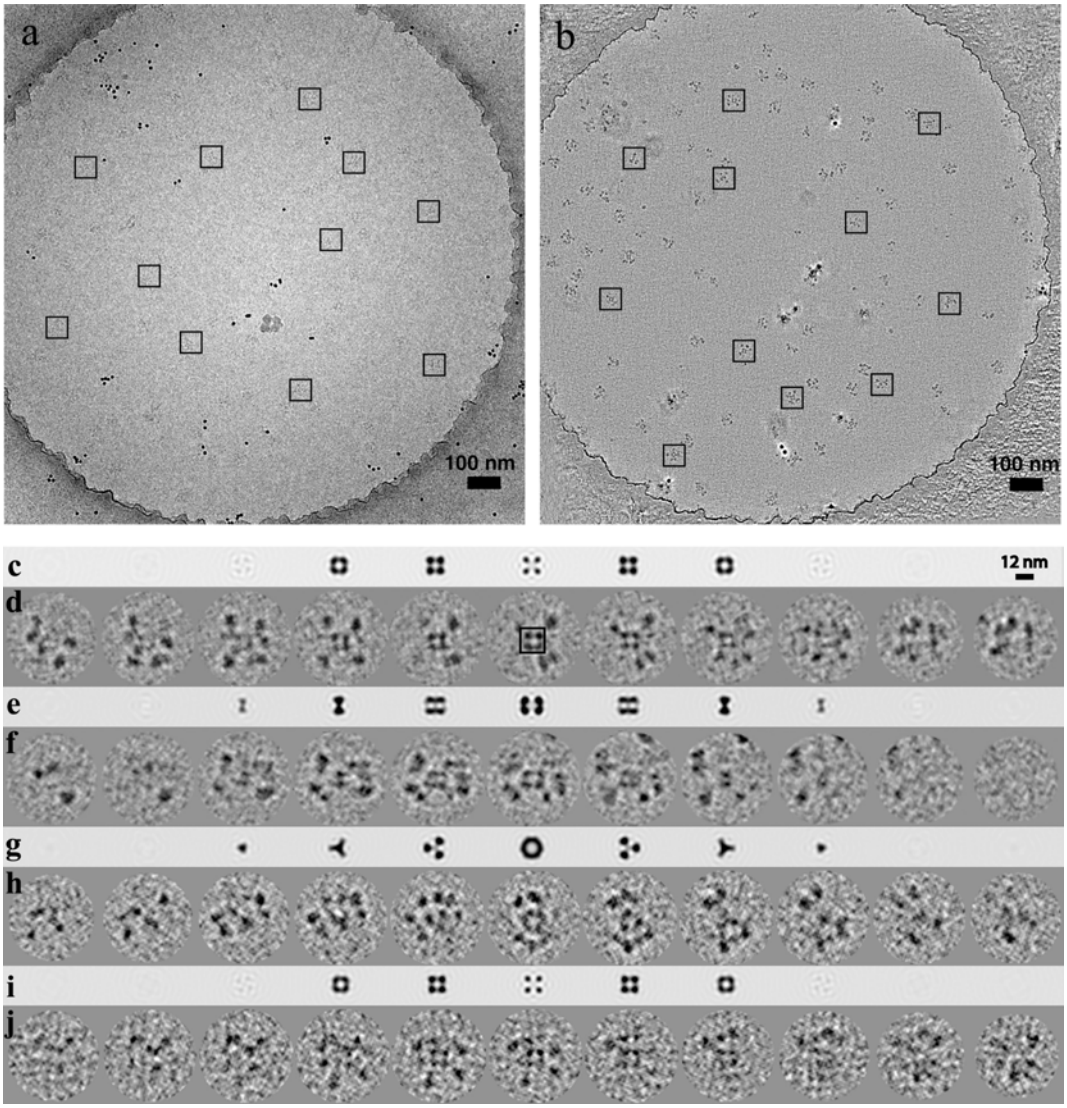

Figure II-1. Raw data and reconstructions

(a) One image from the tomographic tilt series with many PDHC particles boxed in black. The small dark dots are gold fiducials. (b) One 0.82 nm central slice through the three-dimensional reconstruction with particles again boxed. (d, f, h) 2.5 nm thick serial slices through extracted, undenoised PDHC particles that were frozen with their 4-, 2-, and 3-fold axes perpendicular to the plane of the grid, respectively. (c, e, g) 2.5 nm thick

serial slices through a 2.0 nm low-pass filtered map of the E2 crystal structure for comparison, again viewed down the 4-, 2-, and 3-fold axes, respectively. (i, j) Analogous slices through one OGDHC particle frozen with its 4-fold axis perpendicular to the plane of the grid, and its corresponding E2 core crystal structure. A single box drawn in the center of (d) clarifies the region of the reconstructed particles that should be compared to the X-ray structures above. Only in-plane rotations were made to orient the particles in relation to the crystal structure.

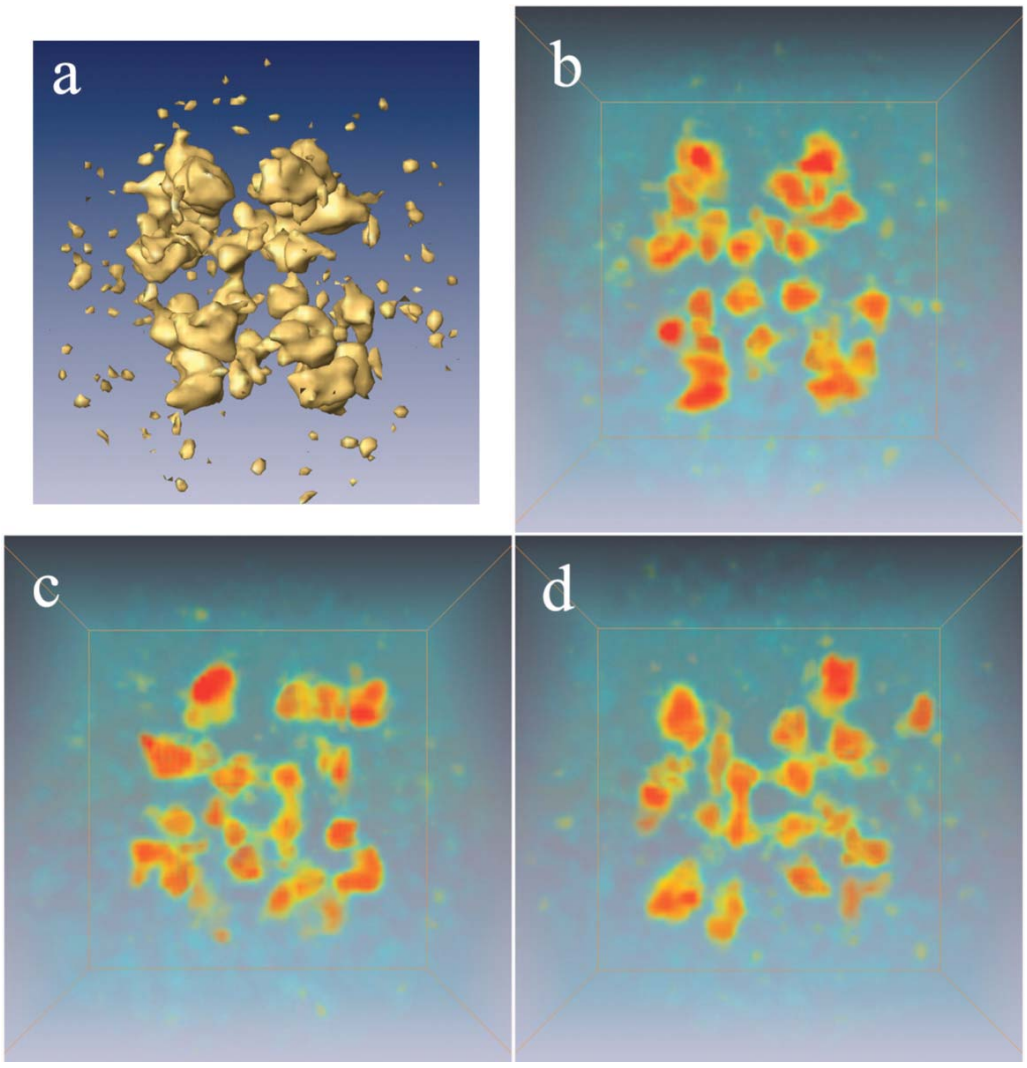

Figure II-2. Particle renderings

(a) Surface rendering of one reconstructed PDHC particle, enclosing the estimated volume of a complete 5.6 MDa complex. (b) Volume rendering of the same particle with the foreground excluded for clarity and to reveal the cubic core. (c-d) Similar volume renderings for two other particles.

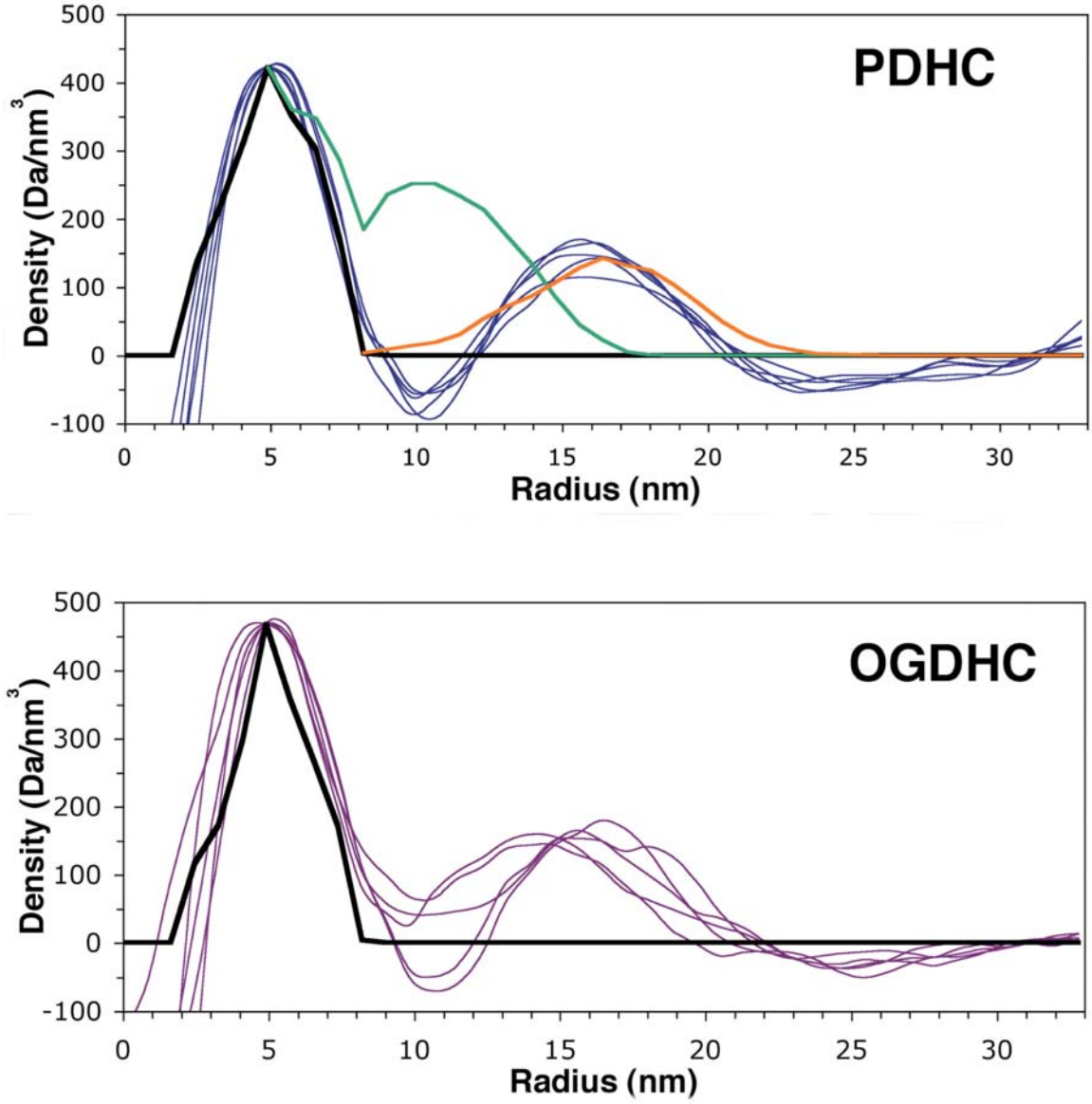

Figure II-3. Radial density plots

Radial density profiles of various atomic models and several reconstructed PDHC (top) and OGDHC (bottom) particles: (blue) five different reconstructed PDHC particles; (purple) five different reconstructed OGDHC particles; (black) the corresponding E2 core crystal structures; (green) face/edge model; (orange) the model produced by manually fitting the atomic structures of E1, E2, and E3 into a single PDHC reconstruction.

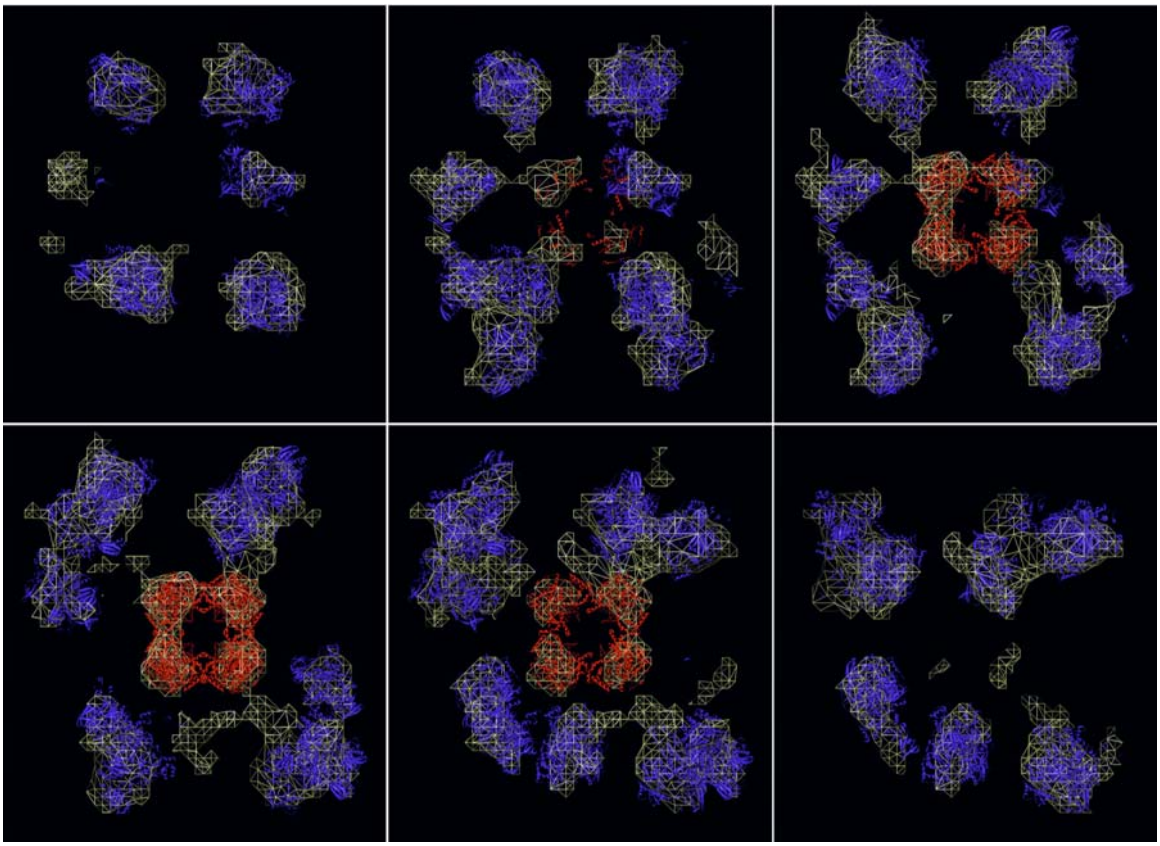

Figure II-4. Resolution as judged by similarity to X-ray crystal structures.

Serial slices through the particle in Fig. II-2a with the roughly fit crystal structures embedded. Crystal structures for the central E2 core and the peripheral E1 or E3 subunits appear in red and blue, respectively. The wire surface again encloses a volume corresponding to a complete complex. The slices are 15 nm thick and overlap each other by 7.4 nm. Note that while the crystal structure of the symmetrically arranged E2 core could be unambigously docked, the resolution was insufficient to distinguish E1 from E3 subunits or their precise orientations. Nevertheless, one set of potential fits are shown to illustrate the clarity of the reconstructions obtained here without any denoising; reconstructed subunits had generally similar sizes and shapes as the crystal structures but could not be docked uniquely.

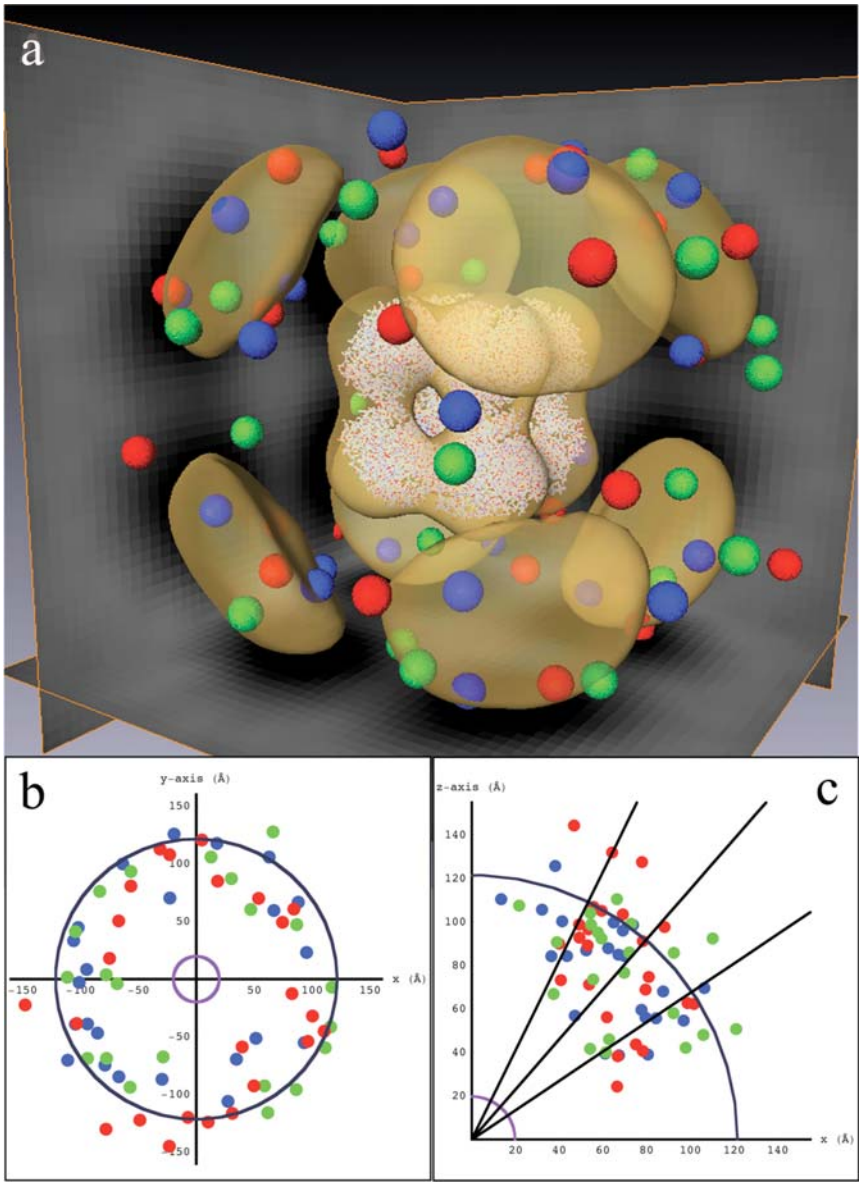

Figure II-5. Random distribution of E1 and E3 around the E2 core

Isosurface of 305 averaged and octahedrally symmetrized reconstructed PDHC particles (yellow), with the E2 crystal structure fit into the core region. Each interpreted E1 or E3 subunit is depicted by a sphere whose radius is approximately one-eighth the true size, colored according to which of the three particles it came from. Individual subunits appear randomly distributed, leading to the amorphous

density directly above the corners of the core in the reconstruction average. (b) Distance and azimuthal angles of the same subunits in relation to their nearest corner. The expected tether lengths of a fully extended polypeptide and a three-dimensional random walk are shown as blue and purple circles, respectively. (c) Distance and polar angles of the centers in relation to their nearest corner, with the same landmark circles as in panel (b). The middle ray depicts the mean polar angle of 41°, while the top and bottom rays delineate the standard deviation of ±15°.

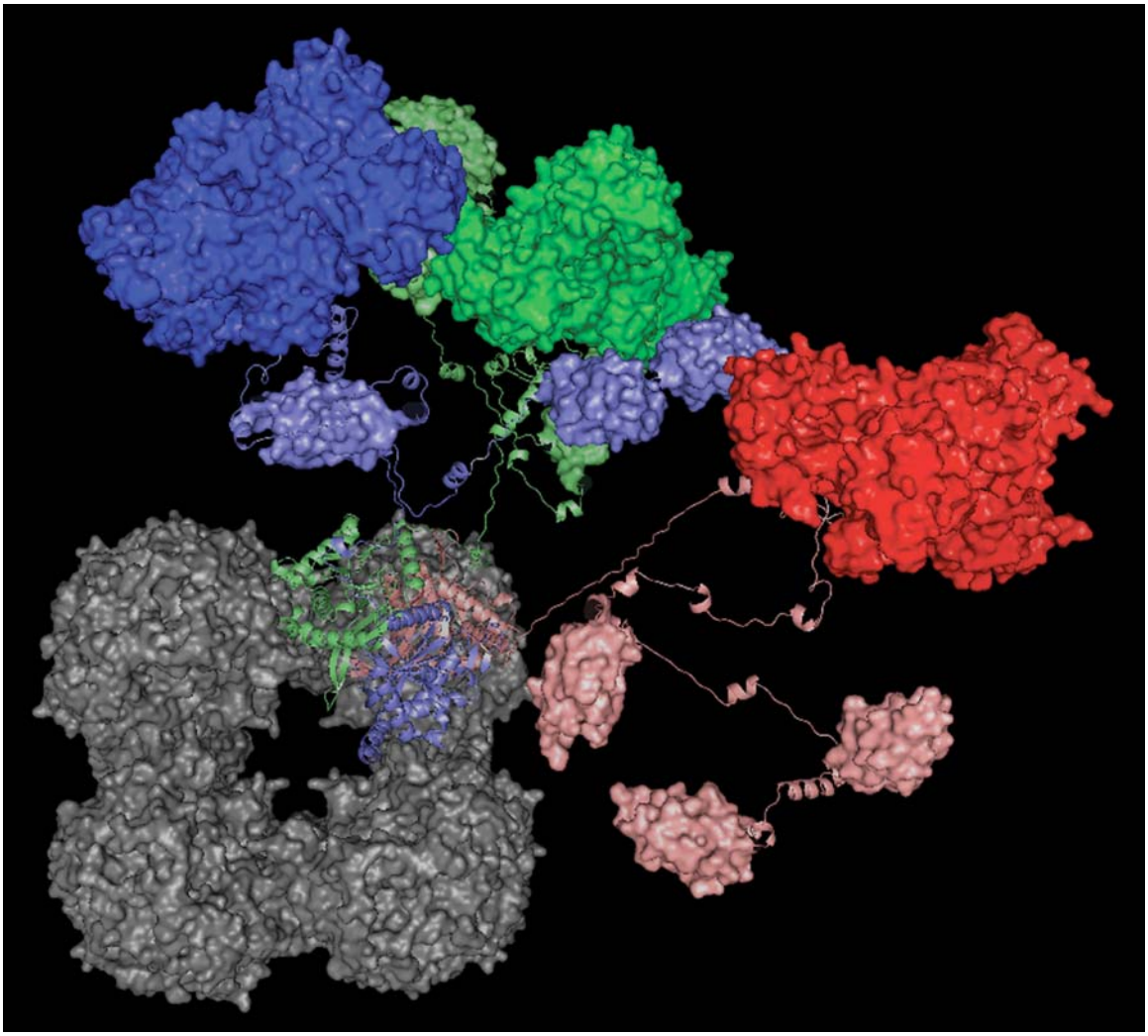

Figure II-6. Complete model of one PDHC corner

One possible conformation of a PDHC corner is depicted. The full E2 core is shown in grey, with the three particular E2 monomers involved in the corner of interest shown in light blue, light green, and pink. Three E3 dimers—correspondingly shown in dark blue, dark green, and red—were positioned according to the density seen above one corner of one particular PDHC reconstruction. The remaining nine lipoyl domains and twelve tethers were placed in reasonable but purely hypothetical positions to provide a sense of the crowdedness in a complete assembly.